Structural basis for the specificity of PPM1H phosphatase for Rab GTPases

Dieter Waschbüsch[1], Kerryn Berndsen[2], Axel Knebel[2], Dario R. Alessi[2†], Amir R. Khan[1,3†]

Addresses:

[1]School of Biochemistry and Immunology, Trinity College Dublin, Dublin 2, Ireland

[2]MRC Protein Phosphorylation and Ubiquitylation Unit, School of Life Sciences, University of Dundee, Dundee, UK and Aligning Science Across Parkinson's (ASAP) Collaborative Research Network

[3]Program in Cellular and Molecular Medicine, Boston Children's Hospital, Boston, USA

[†]Correspondence should be addressed to:

Amir Khan, PhD
Program in Cellular and Molecular Medicine
Boston Children's Hospital
Boston, USA
khan@crystal.harvard.edu

or

Dario Alessi, PhD
MRC Protein Phosphorylation and Ubiquitylation Unit
School of Life Sciences
University of Dundee
Dundee, UK
d.r.alessi@dundee.ac.uk

Running title: PPM1H specificity for Rab GTPases

Abstract

LRRK2 serine/threonine kinase is associated with inherited Parkinson's disease. LRRK2 phosphorylates a subset of Rab GTPases within their switch 2 motif to control their interactions with effectors. Recent work has shown that the metal-dependent protein phosphatase PPM1H counteracts LRRK2 by dephosphorylating Rabs. PPM1H is highly selective and closely related PPM1J/M exhibit virtually no activity toward substrates such as Rab8a phosphorylated at T72 (pT72). Here we have identified the structural determinant of PPM1H specificity for Rabs. The crystal structure of PPM1H reveals a conserved catalytic domain that adopts a β-sandwich fold. The striking difference is that PPM1H has evolved a 110-residue flap domain that punctuates the catalytic domain. The flap domain distantly resembles tudor domains that interact with histones in the context of epigenetics. Cellular assays and 3-D modelling suggest that the flap domain encodes the docking motif for phosphorylated Rabs. Consistent with this hypothesis, a PPM1J chimera with the PPM1H flap domain dephosphorylates pT72 of Rab8a with a higher specific activity than PPM1H. Therefore, PPM1H has acquired a Rab-specific interaction domain within a conserved phosphatase fold.

Keywords: PPM1H phosphatase/LRRK2 kinase/crystal structure/Rab GTPase/membrane trafficking

Introduction

Metal-dependent Ser/Thr phosphatases (PPMs) have a structurally conserved catalytic domain that adopts a β-sandwich fold with Mg^{2+}/Mn^{2+} ions at the active site. Among the family of human enzymes is PPM1A (formerly PP2Cα) which reverses stress-mediated protein kinase cascades [1-3]; PHLPP1/2 which regulates AGC kinases and cellular homeostasis[4]; and pyruvate dehydrogenase phosphatase (PDP1) that is expressed in the mitochondrial matrix and regulates the activity of pyruvate dehydrogenase in metabolism[5, 6]. The core PPM fold, first identified by the structure of PPM1A[7], consists of an 11-stranded β-sandwich flanked on both sides by α-helices. The catalytic cleft is formed on one side of the β-sandwich and comprises a binuclear Mg^{2+}/Mn^{2+} metal center that is coordinated by conserved aspartate residues. The 250-residue PPM fold is better conserved in structure rather than sequence (20-50% identities) across the mammalian enzymes. There is also considerable diversity among PPMs involving the incorporation of sequence elements outside of the catalytic domain. For example, PPM1A has a C-terminal α-helical domain that is not required for catalysis but may contribute to substrate specificity[7-9]. Several enzymes including PPM1A, PPM1B, PPM1K and PDP1 also have a short 50-residue insertion termed the 'flap' subdomain that is poorly conserved in sequence and structure. This region is predicted to contribute to substrate specificity, although chimeric enzymes involving grafts of the flap have not been successful in transferring substrate preference[10]. Studies of bacterial enzymes have proposed a third metal-binding site that contributes to catalysis *via* coordination with a conserved aspartate residue [11-13]. Mutation of the equivalent residue in human PPM1A to alanine (D146A) enabled trapping of a complex of PPM1A with a cyclic phospho-peptide and subsequent structure determination[9].

Recently, PPM1H phosphatase has been identified as the enzyme that counters the LRRK2 signaling cascade by dephosphorylating Rab GTPases[14]. A subset of at least 7 Rabs are physiological substrates of LRRK2[15, 16], a Ser/Thr kinase that is associated with inherited and sporadic forms of Parkinson's disease (PD)[17, 18]. Rabs are members of the Ras superfamily of molecular switches that regulate membrane trafficking in eukaryotes. Rabs oscillate between a membrane-bound GTP form and cytosolic GDP form that is distinguished by local conformational changes in nucleotide-sensitive switch 1 and switch 2 motifs[19]. LRRK2 phosphorylates Rab8a and Rab10 at a conserved threonine residue in their switch 2 α-helix (pT72 in Rab8a). Phosphorylated Rab8a/10 (pRab8a/10) recruit phospho-specific effectors RILPL1 and RILPL2 (Rab interacting lysosomal protein-like 1 and 2) to subcellular compartments downstream of LRRK2 activation. Autosomal dominant PD

mutations that activate LRRK2 kinase interfere with the formation of primary cilia through a pathway involving pRab8a/10 binding to RILPL1[20]. LRRK2 kinase inhibitors have cleared phase 1 for treatment of PD, while alternative strategies to antagonize LRRK2 signaling could be beneficial for future therapeutics.

Here we describe the crystal structure of PPM1H phosphatase which counters the LRRK2 pathway. The structure reveals novel features that have been incorporated into the core catalytic domain. The first is a 110-residue 'flap domain' that is positioned next to the catalytic cleft. This domain is an expansion of the 50-residue flap that is found in other members of the PPM family. The PPM1H flap domain adopts an α/β fold that resembles tudor domains that regulate histone functions in an epigenetic context. On the opposite face of the cleft, a 3-stranded β-sheet motif is also inserted into the core PPM fold. Thirdly, PPM1H has an N-terminal extension that winds behind the active site and inserts into the hydrophobic core of the β-sandwich. This anchor-like interaction has apparently evolved in the PP1H/J/M subfamily of phosphatases as motif that is critical for folding of the enzymes. Mutagenesis, cellular assays and modeling of a phospho-Rab substrate into the active site suggest that the PPM1H flap domain forms a docking site for phosphorylated Rab GTPases. In support of this hypothesis, transfer of the flap domain of PPM1H onto PPM1J is sufficient to convert the PPM1J chimera into a maximally active phospho-Rab8a phophatase. Overall these data reveal that PPM1H phosphatase has evolved substrate specificity through a Rab-specific flap domain within the framework of a conserved catalytic domain.

Results and Discussion

Overall structure of PPM1H phosphatase

Full-length PPM1H expressed in *E.coli* cells was unstable and prone to degradation. To design a crystallisable protein, the N-terminal residues 1-32 were eliminated due to predicted flexibility. We also introduced a D288A mutation ($PPM1H^{DA}$) that destabilizes a third metal (Mg^{2+}/Mn^{2+}) at the active site [9]. Crystals were grown of $PPM1H^{DA}$ that diffracted to 3.1 Å resolution, but no crystals grew of the WT variant. To grow WT crystals and improve diffraction, a 'loop deletion' variant of PPM1H (PPM1H-LD) was designed to eliminate a flexible loop (188-226) that was predicted to be distant from the active site (**Fig 1A**). WT and D288A variants of PPM1H ($PPM1H^{wt}$-LD, $PPM1H^{DA}$-LD) diffracted to 2.5 Å and 2.6 Å resolution, respectively. The 3 variants $PPM1H^{DA}$, $PPM1H^{wt}$-LD, and $PPM1H^{DA}$-LD have identical 3-D structures with two Mg^{2+} ions at the active site, and they all begin at residue S33. Therefore the 2.5 Å structure of $PPM1H^{wt}$-LD can be used as a model for ensuing discussions. Deletion of the loop 188-226 and the N-terminus (1-32) does not affect the ability of $PPM1H^{wt}$-LD to dephosphorylate pRab8a relative to the full-length enzyme (**Fig EV1A**).

The structure of PPM1H adopts a conserved PPM fold that consists of 10 β-strands organized into a 5x5 β-sandwich (**Fig 1B**). The first β-sheet comprises β-strands β2, β7, β8, β10 and β11. The second β-sheet consists of β-strands β3, β4, β5, β6, and β9. Two α-helices pack against the each of the two concave surfaces of the β-sandwich. The long and curved α-helices α1 and α2 are oriented in an anti-parallel manner and pack against the second β-sheet. The shorter helices α4 and α5 are also oriented in an anti-parallel fashion and pack against the first β-sheet. The active site cleft is formed by loops, including a short α-helical loop (α4, residues 443-447), that connect β-strands on one edge of the β-sandwich. Three conserved aspartate residues – D151, D437 and D498 – form direct contacts with two Mg^{2+} ions (M1 and M2) at the active site. M1 is coordinated by D437 and D498, while D151 coordinates both metal sites. The metal binding includes water molecules and the geometry is approximately octahedral for both metal sites (M1 and M2). A structure-based sequence alignment of PPM family enzymes is shown with secondary structures and other annotated features (**Fig EV1B**).

One of the distinctive features of PPM1H is a 110-residue flap domain that adopts an α/β fold (**Fig 1C**). All known structures of human PPMs (PPM1A, PPM1B, PPM1K and PDP1) have a shorter 50-residue flap that is inserted between the terminal β-strands of the two β-sheets (β8 and β9 in PPM1H). In PPM1H, this domain comprises an α-helix that stacks against a highly twisted β-sheet. This

extended flap domain effectively creates a large surface adjacent to the active site for potential substrate recognition. Matching of the flap domain to structures in the DALI server [21] reveals a resemblance to the tudor domain despite the absence of sequence similarities (**Fig 1C**). Tudor domains are also composed of an α-helix that stacks against a highly twisted anti-parallel β-sheet. These domains are involved in the recognition of methylated lysine or arginine residues of histones *via* an aromatic cage. Although roughly similar in appearance, the α/β subdomain of PPM1H has a different topology and lacks characteristic structural motifs such as the aromatic cage that are common to tudor domains. Despite flap sequence and structural diversity among the PPM family, a short loop that packs against the catalytic domain is highly conserved in sequence and conformation (dotted circle, **Fig 1C**). This region is discussed in investigated in more detail below.

Substrate docking and mutagenesis suggest roles for the flap domain in catalysis

Phosphorylated Rab8a (pRab8a, GTP-bound) from the recent structure of the pRab8a:RILPL2 complex[22] was manually docked onto PPM1H to identify possible determinants of substrate specificity and catalysis (**Fig 2A**).The structure of PPM1A in complex with a cyclic phosphopeptide[9] was used to guide pT72 of pRab8a into the active site. Energy minimization was not performed, therefore our hypothetical model shows the uncomplexed conformation of PPM1H with a model substrate. The flap domain and the β-sheet motif have the effect of expanding the size of the binding cleft relative to known structures of PPM phosphatases. The modeling suggests that the dimensions of pRab8a are compatible with the size of the active site cleft. There are minor clashes between the flap domain and the switch 1 region of pRab8a. In addition, the C-terminal part of the switch 2 helix clashes modestly with the β-sheet motif on the other side of the cleft. These steric conflicts may be overcome through rigid body motions of these regions in the genuine complex. From the modeling, we identified R338 is a potential site of pRab8a binding despite being located 27 Å from the catalytic Mg^{2+} ions. In addition, a loop in the flap domain that forms an interface with α2 and the β-sandwich of the catalytic domain was intriguing (**Fig 1B**). Despite the diversity of flap regions in the PPM family, a short motif in this loop is highly conserved in sequence and conformation (**Fig 2A**). Finally, a lysine residue (K88) was identified which is conserved as R33 in PPM1A and is expected to bind directly to the phosphate moiety of substrates[9].

We firstly evaluated the impact of the K88A and R338A mutations in a quantitative biochemical timecourse assay using either pT72-Rab8a complexed to GTPγS as a substrate (**Fig 2B**, left) or a peptide substrate (AGQERFRT*ITTAYYR) that encompasses residues 65 - 79 of human Rab8a

phosphorylated at T72 residue (**Fig 2C**, right). For these assays, full-length PPM1H variants with an N-terminal SUMO tag were purified (**Fig EV2A**). Although there are impurities in these preparations, their levels relative to intact enzyme are similar among the WT and mutants. The exception was L392A whose low yield of intact enzyme precluded quantitative analyses. The assays revealed that the PPM1H[K88A] mutation reduced initial rate activity by over 20-fold using both peptide and protein substrates. This is consistent with K88 playing a key role in mediating a direct contact with phospho-threonine of substrates. The R338A mutation reduced PPM1H initial activity around 2-fold when assayed with the phospho-Rab8a protein (**Fig 2B**, left) but had no significant impact when assayed with the phsopho-Rab8a peptide (**Fig 2B**, right). This result is consistent with R338 in the flap domain contributing towards optimal docking of pRab8a protein substrate, but not the peptide.

Using an HEK293 cell assay, we next investigated the role of the conserved loop from the flap domain which forms an interface with the catalytic core (**Fig 2C**). The L392A mutant was expressed at slightly lower levels compared to wild type and displayed reduced activity towards phosphorylated Rab10. We also generated a quadruple (L392A+D394A+H395A+D396A) that eliminates several interactions simultaneously between the loop and the catalytic domain. When expressed in HEK293 cells, this quadruple mutant lacked detectable activity towards phosphorylated Rab10 and was expressed ~2-fold lower levels that wild type PPM1H (**Fig 2C**). Therefore, this conserved loop in the flap domain likely contributes to folding and/or catalysis. We also assessed the impact of K88A and R338A mutations in this less quantitative HEK293 cell assay and observed that both mutations were expressed at comparable levels to wild type with partially reduced ability of PPM1H to dephosphorylate Rab10 (**Fig 2C**).

It is unknown whether PPM1H dephosphorylates pRab8a in its GTP or GDP state. To address this question, we generated pRab8a complexed to GDP or GTPγS and undertook K_m/V_{max} kinetic analyses (**Fig 2D**). This revealed that PPM1H dephosphorylated both the GDP and GTPγS phospho-Rab8a with moderately different kinetics. PPM1H dephosphorylated the GDP-phospho-Rab8a complex with a K_m of 24 μM and a V_{max} of 3.0 μM/min and GTP-phospho-Rab8a complex with a K_m of 14 μM and a V_{max} of 1.4 μM/min. Therefore, the V_{max} is doubled for the GDP complex, but the GTP complex is dephosphorylated with an ~40% lower K_m. This suggests that PPM1H *in vivo* would be able to act on both the GTP and GDP locked phospho-Rab proteins.

Anchor-like folding motif in the PPM1H/J/M subfamily

PPM1H has a novel N-terminal extension preceding the core PPM fold (**Figs 3A**). S33 interacts with the C-terminus of α2, adjacent to the flap domain, before winding around the back of the enzyme to the opposite side of the β-sandwich. PPM1A and PDP1 have an additional β-strand (β1) at the edge of the first β-sheet. In PPM1H, part of this anti-parallel β1 strand is conserved, while the remainder appears to be dislodged and forms a loop preceding a shortened β2 strand. This distinct conformation of PPM1H is a consequence of the insertion of hydrophobic residues from a short 3_{10} helix. This conformation facilitates the insertion of the aromatic ring of F46 into the hydrophobic core of the β-sandwich (**Fig 3A**). Resembling an 'anchor', the side chains of P44, F46, and L47 cap the hydrophobic core of the β-barrel, effectively substituting for strand β1. Systematic deletion of the N-terminal residues of PPM1H toward the anchor residues also appears to disrupt folding as judged by reduced expression in HEK293 cells and loss of activity towards LRRK2 phosphorylated Rab10 (**Fig 3B**). Strikingly, PPM1H is relatively active until R43 is deleted (construct 44-end). To probe the importance of these residues we mutated P44, F46 and L47 to Ala and observed that this nearly abolished PPM1H soluble expression in HEK293 cells, emphasizing their importance for enzyme folding (**Fig EV2B**). Following these hydrophobic interactions, an α-helix (N51-A58) and loop (D59-I65) interact directly with an active site loop (V83-D94).

Despite sequence diversity at their N-termini, the PPM1H/J/M subfamily of phosphatases have a conserved RPxFL motif (**Fig 3C**). This anchor motif is likely involved in the folding of the catalytic domain through hydrophobic interactions with the β-sandwich. It may also influence catalysis due to its protrusion against the active site and its tether-like connection between the flap domain and the β-sheet motif.

PPM1J chimeras with the PPM1H flap domain are active against pRab8a

Although PPM1J is the closest relative to PPM1H, previous work revealed negligible activity towards LRRK2 phosphorylated Rabs in cellular or biochemical assays[14]. Ignoring loops that are predicted to be unstructured and distant from the active site cleft, PPM1H and PPM1J have an identical domain organization (**Fig 4A**). Mapping of PPM1H/J sequence conservation onto the structure of PPM1H suggest that residues in the core PPM domain that line the catalytic cleft are strongly conserved. Therefore, the catalytic domain is unlikely to account for Rab specificity. However, the flap domain and the N-terminal region comprising the anchor diverge significantly relative to the active site (**Fig 4B, Fig EV4**).

To further explore the determinants of specificity, we engineered PPM1J chimeras that adopt the PPM1H anchor and/or flap domain (**Fig 5A**). The structure of PPM1H was critical for guiding the sites for grafts and thereby maintaining the integrity of the core catalytic fold. We evaluated the effects of domain swapping on the ability of PPM1J to dephosphorylate pRab8a in our biochemical assays. Strikingly, the PPM1J chimera proteins containing the PPM1H flap domain were markedly active towards the pRab8a protein displaying ~2-fold higher specific activity compared to wild type PPM1H (**Fig 5C,** *left panel*). We also noted that the PPM1J chimera proteins containing the PPM1H flap domain restored and further increased ~2-fold the activity towards the phospho-Rab8a peptide substrate (**Fig 5C**, *right panel*). This indicates that a portion of the PPM1H flap domain is also contributing to the interaction with the phospho-peptide. PPM1J displayed detectable but low activity towards the T72-phosphorylated Rab8a peptide. In contrast, the PPM1J chimera possessing the PPM1H N-terminal anchor displayed very low activity towards the pRab8a protein or peptide substrate similar to PPM1J. It should be noted that the PPM1J chimera possessing the PPM1H anchor did display higher activity than wild type PPM1J when assayed with the phospho-Rab8a protein (**Fig 5C,** *left panel*), suggesting that this region could make a minor contribution towards substrate specificity. Comparable activities of the J/H double and J/H flap chimeras suggest that the anchor regions of PPM1H/J can be swapped without effects on catalysis. Overall, these data suggest that PPM1H specificity for pRab8a is principally mediated by the flap domain of PPM1H.

Model for PPM1H specificity for Rab GTPases

The PPM family of phosphatases have a common catalytic domain with the incorporation of diverse structural elements that facilitate their specificity and function. The flap region, adjacent to the active site, is poorly conserved in sequence and structure in the PPM family. It has been associated with substrate specificity[13], but previous chimeras involving the flap region have been unsuccessful in transferring functions [10]. Here we provide evidence that PPM1H phosphatase specificity for Rab GTPases is encoded by the flap domain (**Fig 5D**). Substitution of this domain into PPM1J leads to its ability to hydrolyze phospho-Rab8a more efficiently that PPM1H. Also, we have identified a highly conserved loop motif from the flap domain that appears to contribute to folding and/or catalysis. This conserved loop in human PPMs has not been investigated previously. Although speculative, we suspect that it could couple substrate binding to catalysis given its proximity to the active site. Intriguingly, the equivalent L392 hydrophobic pocket has recently been identified as a 'regulatory switch' in bacterial phosphatases[23]. Finally, an anchor motif preceding the catalytic domain interacts with the hydrophobic core and contributes to enzyme folding/catalysis.

Although these extended flap domains are conserved in evolutionarily related PPM1J and PPM1M, subtle differences in their sequences and/or conformations likely encode the exquisite specificity of PPM1H for phosphorylated Rab8a/10. PPM1H has been localized to Golgi, where it likely counters the LRRK2 pathway by dephosphorylating Rab8a and Rab10 under physiological conditions[14]. Rab proteins have a flexible stretch of ≈30 residues between their G domain and their prenylated C-terminal tails that localize them to subcellular membranes (**Fig 5D**). In future work it would be important to dissect the mechanism by which PPM1H localizes to membranes. It would also be important to try and capture the complex between phospho-Rab and a substrate trapping mutant of PPM1H to fully understand specificity and catalysis.

Materials and Methods

Constructs and expression of proteins

The cDNA for PPM1^{DA}-LD (residues 33-514, D288A) with the residues 188-226 replaced by a short GSGS motif was synthesized as a codon-optimized gene for *E. coli* expression (Genscript, Inc). The cDNA was cloned into pET28a-(+)-TEV at the NdeI/BamH1 restriction sites. The PPM1H^{wt}-LD construct was made by site directed mutagenesis using the following primers: 5'-GTG GCG AAC GCG GGT GAT AGC CGT GCG ATC ATT ATC-3' (for) and: 5'-GAT AAT GAT CGC ACG GCT ATC ACC CGC GTT CGC CAC-3' (rev). Full-length and 57-end cDNA variants of PPM1J were obtained from Genscript with codon-optimization for *E.coli* expression. Using NdeI and BamH1 sites at their 5' and 3' ends, the genes were inserted into the same vector above. The PPM1H^{DA} (residues 33-514) construct was amplified using the following primers: 5'-TACTTCCAATCC <u>TCG</u> GAC CTG CCC CTG CGT TTC3' (for) and 5'-TATCCACCTTTACTG <u>TTA TCA</u> TGA CAG CTT GTT TCC ATG-3' (rev); S33(PPM1H)/stop codons underlined. We used a human PPM1H (NM_020700) template carrying the D288A mutation and LIC cloned the resulting DNA into the pNIC28-BSA4 vector which allows the expression of a hexahistidine -tagged protein. All plasmids generated by PCR were confirmed by sequencing.

Expression of PPM1H was carried out in LB Broth supplemented with 30 µg/ml kanamycin (FORMEDIUM™). After incubation at 37°C to an OD_{600} of ~0.6 the culture was cooled down to 18°C and induced with 0.5 mM IPTG (FORMEDIUM™), after which cells were grown at 18°C overnight. Cells were harvested by centrifugation and the pellets were resuspended in His-tag extraction buffer (20 mM Tris-HCl pH 8.0, 300 mM NaCl, 5 mM $MgCl_2$, 20 mM imidazole and 10 mM β-mercaptoethanol). After lysis by sonication the cell lysate was centrifuged at 26,000 x g for 45 minutes at 4°C to remove cellular debris. The supernatants were loaded onto a nickel agarose resin (QIAGEN) in a gravity flow setup. The resin was washed with a 10-fold excess of extraction buffer and 5-fold excess wash buffer (extraction buffer supplemented with 40 mM Imidazole). The hexahistidine-tagged protein was then eluted using extraction buffer supplemented with 200 mM imidazole.

Removal of the His_6 tag was performed by overnight incubation at 4°C in dialysis against gel filtration buffer (20mM Tris-HCl pH 8.0, 100mM NaCl, 5mM $MgCl_2$, 1mM DTT) using recombinant TEV protease, followed by a second Ni^{2+}-agarose column. The 'flow-through' fractions were collected, while the uncut proteins remained on the resin. Soluble aggregates were eliminated by running the

sample through a Superdex 200 (10/300) gel filtration column (GE Healthcare) equilibrated in gel filtration buffer. The peak fractions of PPM1H were pooled and concentrated in 10kDa MWCO concentrator tubes prior to crystallization trials.

Phosphorylation of Rab8a Q67L

The *in vitro* phosphorylation of Rab8a (T72) by MST3 kinase and subsequent purification has been described previously[22]. In brief, Rab8a was mixed with MST3 at a 8:1 molar ratio, and incubated overnight. The phosphorylation buffer was adjusted to the following conditions: 50mM Tris-HCl, 150mM NaCl, 10mM $MgCl_2$, 2mM ATP, pH 7.5. The phosphorylation mixture was then dialyzed against low salt buffer and loaded to a MonoS (GE HEalthcare) column. Phosphorylated Rab8a was separated from unphosphorylated by ion exchange chromatography applying a 50% gradient low to high salt buffer (10mM MES, 10mM (low) or 1M NaCl (high), 5mM $MgCl_2$, 1mM DTT, pH 5.2). The phosphorylation of Rab8a was confirmed by PhosTag gel electrophoresis prior to subsequent experiments.

Crystallization, data collection and refinement

Crystals of PPM1H variants were grown at concentrations between 5-10 mg/L using the vapour diffusion method. Crystals were harvested in precipitant supplemented with 30% glycerol and stored frozen in liquid nitrogen. X-ray data were collected under a cryogenic nitrogen stream (100K) at the FMX beamline, NSLSII synchrotron (Brookhaven, New York, USA). Details of crystallization conditions and the quality of diffraction data are shown in **Table 1**. Native diffraction data were reduced using XDS and aimless, followed by structure determination using the Phaser software in the PHENIX package[24, 25]. Molecular replacement using Phaser (PPM1A; PDB code 6b67[9]) was successful using data from crystals of $PPM1H^{DA}$-LD, and subsequently, Autobuild in Phenix provided an initial model for PPM1H. Refinement was performed through multiple rounds of energy minimization and model building using Phenix and Coot software[26]. The structures of the other variants of PPM1H ($PPM1H^{wt}$ AND $PPM1H^{WT}$-LD) were determined using $PPM1H^{DA}$-LD as a search model and subsequently refined using Phenix and Coot. These higher resolution models were useful for the final refinement of $PPM1H^{WT}$-LD within several loops and the flap domain. To reduce model bias, all three structures have the same reflections flagged for the R-free set. The asymmetric unit for all structures contains two molecules of PPM1H, each with two magnesium ions. Two non-native residues (His-Met) from the cleaved affinity tag are seen in one of the molecules of $PPM1H^{DA}$-LD at its N-terminus. Statistics from the refinement are shown in **Table 1**.

Antibodies

Antibodies			
anti-HA (clone 3F10) (Rat IgG1)	Sigma-Aldrich	11867423001	WB (1:1000)
anti-phospho-Rab10 (Thr73) (Rabbit monoclonal)	Abcam	#ab23026	WB (1:1000)
anti Rab10 (mouse monoclonal)	nanotools	0680-100/Rab10-605B11	WB (1:1000)
anti-LRRK2 (mouse monoclonal)	Neuromab	75-253	WB (1:1000)
anti-phospho-LRRK2 (Ser935) (rabbit monoclonal)	MRC PPU	UDD2	WB (1:1000)

Plasmids for expression in HEK293 cells

Expression constructs were obtained from the MRC-PPU repository at the University of Dundee:

Plasmids:

DU number	cDNA construct (pCMV5D)
DU44059	HA-Empty
DU13077	FLAG-LRRK2 [R1441G]
DU44250	HA-Rab10
DU62789	HA-PPM1H WT
DU62928	HA-PPM1H [H153D]
DU62985	HA-PPM1H [D288A]
DU68360	HA-PPM1H loopDEL
DU68361	HA-PPM1H loopDEL [D221A]
DU68435	HA-PPM1H [F46A]
DU68463	HA-PPM1H [P44A/F46A/L47A]
DU68433	HA-PPM1H [K88A]
DU68422	HA-PPM1H [R338A]
DU66371	HA-PPM1H [L392A]
DU66380	HA-PPM1H [L392A/D394A/H395A/D396A]
DU61295	HA-PPM1H [D394A]
DU61297	HA-PPM1H [H395A]
DU61298	HA-PPM1H [D396A]
DU68393	HA- PPM1H 62-end
DU68394	HA-PPM1H 74-end
DU68077	HA-PPM1J WT
DU70010	HA-PPM1J/H Chimera
DU61258	HA-PPM1H 38-end
DU66542	HA-PPM1H 39-end
DU66546	HA-PPM1H 40-end
DU66543	HA-PPM1H 41-end
DU66544	HA-PPM1H 42-end
DU66545	HA-PPM1H 43-end
DU61350	HA-PPM1H 44-end
DU61260	HA-PPM1H 45-end

DNA constructs were amplified in *Escherichia coli* DH5α and purified using a Hi-Speed Plasmid Maxi Kit (Qiagen).

Cell culture, transfections, treatment, and lysis

HEK293 cells were cultured in Dulbecco's modified Eagle medium (Gibco) supplemented with 10% (v/v) foetal bovine serum, 100 U/ml penicillin and 100 µg/ml streptomycin at 37°C and 5% CO2. Cells used in this study were regularly tested for mycoplasma contamination. Transient transfections were performed 24 h prior to cell lysis using polyethylenimine PEIMax (0.1% w/v) (Polysciences)[27]. Cells were grown to ~70% confluency in 6-well (3.5 cm well diameter) plates prior to transfection. 1.75 µg total plasmid DNA was mixed with 5.5 µl PEI in 150 µl Opti-MEM I Reduced Serum Media (Gibco) and incubated for 30 min at room temperature. The DNA-PEI mixture was added drop-wise to cells. Cells were treated ± MLi-2 LRRK2 inhibitors[28] at a final concentration of 200 nM 90 min prior to lysis. Cells were lysed in 150 µl ice-cold lysis buffer (50 mM Tris-HCl pH 7.5, 150 mM NaCl, 10% glycerol, 10 mM 2-glycerophosphate, 10mM sodium pyrophosphate, 1 mM sodium orthovanadate, 1 µg/ml microcystin-LR, complete EDTA-free protease inhibitor cocktail (Roche), and 1% (v/v) Triton X-100) and collected in 1.5 ml Eppendorf tubes. Lysates were clarified by centrifugation at 20 800 *g* at 4°C for 20 min and supernatants were quantified by Bradford assay before subjected to immunoblot analysis.

Immunoblot analysis

Clarified cell or tissue extracts were mixed with a quarter of a volume of 4× SDS–PAGE loading buffer [250 mM Tris–HCl, pH 6.8, 8% (w/v) SDS, 40% (v/v) glycerol, 0.02% (w/v) Bromophenol Blue and 4% (v/v) 2-mercaptoethanol]. 10-30 µg of samples were loaded onto NuPAGE 4–12% Bis–Tris Midi Gel (Thermo Fisher Scientific, Cat# WG1403BOX) and electrophoresed at 130 V for 2 h with the NuPAGE MOPS SDS running buffer (Thermo Fisher Scientific, Cat# NP0001-02). At the end of electrophoresis, proteins were electrophoretically transferred onto the nitrocellulose membrane (GE Healthcare, Amersham Protran Supported 0.45 µm NC) at 100 V for 90 min on ice in the transfer buffer (48 mM Tris–HCl and 39 mM glycine). Transferred membrane was blocked with 5% (w/v) skim milk powder dissolved in TBS-T [20 mM Tris–HCl, pH 7.5, 150 mM NaCl and 0.1% (v/v) Tween 20] at room temperature for 1 h. The membrane was typically cropped into three pieces, namely the 'top piece' (from the top of the membrane to 100 kDa), the 'middle piece' (between 100 and 37 kDa) and the 'bottom piece' (from 37 kDa to the bottom of the membrane). The top piece was incubated with rabbit anti-LRRK2 pS935 UDD2 antibody multiplexed with mouse anti-LRRK2 C-terminus total antibody diluted in 5% (w/v) bovine serum albumin in TBS-T to a final concentration of 1 µg/ml for each of the antibody. The middle piece was incubated with rat anti-HA antibody diluted in 5% (w/v) bovine serum albumin in TBS-T to a final concentration of 50 ng/ml. The bottom pieces were incubated with mouse anti-GAPDH multiplexed with rabbit MJFF-pRab10-clone-1 monoclonal

antibody and rat anti-HA antibody diluted in 5% (w/v) bovine serum albumin in TBS-T to a final concentration of 0.5 µg/ml for each of the antibody. All blots were incubated in primary antibody overnight at 4°C. Prior to secondary antibody incubation, membranes were washed three times with TBS-T for 10 min each. The top and bottom pieces were incubated with goat anti-mouse IRDye 680LT (#926-68020) secondary antibody multiplexed with goat anti-rabbit IRDye 800CW ((#926-32211) secondary antibody diluted in TBS-T (1:25, 000 dilution) for 1 h at room temperature. The middle piece was incubated with goat anti-mouse IRDye 800CW (#926-32210) secondary antibody diluted in TBS-T (1 : 25, 000 dilution) at room temperature for 1 h. Membranes were washed with TBS-T for three times with a 10 min incubation for each wash. Protein bands were acquired via near infrared fluorescent detection using the Odyssey CLx imaging system and quantified using the Image Studio software.

***E.coli* expression and purification of recombinant phosphatases**

Plasmids (DU62835; DU68087; DU68140; DU68554; DU68559; DU68560; DU68621; DU68625; DU70009, all available from MRC-PPU Reagents: mrcppureagents.dundee.ac.uk) were transformed into *Escherichia coli* BL21-DE3-pLysS and expressed in 3 x 11 litre of Lucia Broth medium (Merck) supplemented with 100µg/ml ampicillin (Formedium). Bacteria were cultured at 37°C until OD600 reached 0.8. The temperature was reduced to 16°C and after 1 h protein phosphatase expression was induced by addition of 25 µM Isopropyl β-D-1-thiogalactopyranoside for incubation overnight. Cells were harvested by centrifugation at 4200 x g for 30 min at 4°C before being resuspended in 20ml collection buffer (50 mM Tris-HCL pH 7.5, 150 mM NaCl, 20 mM imidazole, 2 mM $MgCl_2$, 7 mM 2-mercaptoethanol). The resuspension was made to 5% (by vol) glycerol, 300 mM NaCl, 0.4% Triton X-100, 1 mM AEBFS (Pefabloc®), and 10 µg/ml Leupeptin. Cell suspension was sonicated, and insoluble material was removed by centrifugation at 40,000 x g at 4°C for 25 min. 2ml Cobalt resin was equilibrated in collection buffer before incubated with lysates for 2 h at 4°C. After incubation, resin was washed 5 times with 7 volumes wash buffer (50 mM Tris-HCL pH 7.5, 250 mM NaCl, 20 mM imidazole, 2 mM $MgCl_2$, 7 mM 2-mercaptoethanol, 5% (v/v) glycerol). The resin was transferred onto a 5 ml polyprep (Biorad) filtration device. Protein was eluted with elution buffer (wash buffer diluted with 1 M imidazole to 0.4 M imidazole) and 1 ml fractions were collected. Protein-containing fractions were pooled and 1.6 ml protein was subjected to size exclusion chromatography using a Superdex 200 XK16/60 column (GE Healthcare) and equilibrated into 50 mM Tris-HCL pH 7.5, 200 mM NaCl, 2 mM $MgCl_2$, 7 mM 2-mercaptoethanol, 0.015% (w/v) Brij35. Fractions containing PPM1H were pooled and concentrated before aliquoted and snap frozen to store at -80°C.

Quality control gel for recombinant phosphatases

3 μg of each protein was prepared in SDS-PAGE sample buffer and 5% 2-mercaptoethanol. Electrophoresis was carried out using NUPAGE Bis-Tris 4-12% gradient gels (Life Technologies) and run at 120 V. The gel was then stained for 1h using Instant Blue Coomassie (Expedeon). Protein concentrations were adjusted using the upper protein band, which corresponded to the undegraded protein.

Quantitative phosphatase assays

The quantitatively Thr72 phosphorylated Rab8A complexed to either GTP or GDP was prepared as described previously[14]. The phosphopeptide encompassing the Thr72 LRRK2 phosphorylation site on human Rab8A (AGQERFRT*ITTAYYR residues 65 – 79, where T* - pThr) was synthesized and purified by JPT Peptide Technologies GmbH. Phosphate release from either the phospho-Rab8A protein or peptide was detected by using the malachite green phosphatase assay[29] according to the sigma protocol. The phosphatase assays were performed in 96-well flat bottomed plates using a final volume of 80 μl and either 25 nM PPM phosphatase and 16 μM phospho-Rab8A protein or 50 nM PPM phosphatase and 32 μM phospho-Rab peptide. The phosphatase was diluted in 50 mM Tris-HCl pH 7.5, 200 mM NaCl, 2 mM $MgCl_2$, 7 mM 2-mercaptoethanol, 5% (v/v) glycerol. The phospho-Rab8A protein and phospho-peptide are diluted in 40 mM HEPES buffer pH7.5, supplemented with 10 mM $MgCl_2$ at a final reaction volume of 80 μl. The reactions were undertaken at room temperature and initiated by adding the diluted phosphatase to the phospho-Rab8A protein or phospho-peptide substrate. At the indicated times the reactions were quenched by addition of 20 μl Malachite Green working reagent (Sigma Aldrich; MAK307). After incubation at room temperature for 30 min absorbance was measured at 620 nm. Free phosphate at increasing concentrations (1-40 μM) was used to make a standard curve, and used to determine the concentration of phosphate released from each reaction. Malachite green working reagent and free phosphate standards were prepared fresh prior to each experiment, according to Sigma manual. Graphs were prepared using GraphPad Prism 5 software. To determine Km and Vmax of PPM1H against substrate Rab8a, phosphatase reactions were analyzed as described above except that the concentrations of phospho-Rab8a protein complexed to either GDP or GTPγS were varied between 2-32 μM. The initial rate (V_0) was calculated by dividing concentration of released phosphate at 5 min by time and plotted against each substrate concentration. Enzyme kinetic constants were then obtained using GraphPad Prism 5 software.

Acknowledgements

We thank Pawel Lis for helpful discussion and advice, the excellent technical support of the MRC-Protein Phosphorylation and Ubiquitylation Unit (PPU) DNA Sequencing Service (coordinated by Gary Hunter), the MRC-PPU tissue culture team (coordinated by Edwin Allen), MRC PPU Reagents and Services antibody and protein purification teams (coordinated by Hilary McLauchlan and James Hastie). We thank Suzanne Pfeffer for helpful advice and discussions.

Funding

A.R.K. was supported by the Program for Cellular and Molecular Medicine, Harvard Medical School. D.R.A is funded by the joint efforts of The Michael J. Fox Foundation for Parkinson's Research (MJFF) [17298] and Aligning Science Across Parkinson's (ASAP) initiative. MJFF administers the grant (ASAP-000463) on behalf of ASAP and itself, UK Medical Research Council [grant number MC_UU_12016/2 (D.R.A.)] and the pharmaceutical companies supporting the Division of Signal Transduction Therapy Unit (Boehringer-Ingelheim, GlaxoSmithKline, Merck KGaA -to D.R.A.).

Intellectual property rights notice: "This research was funded in part by Aligning Science Across Parkinson's [Grant ID: ASAP-000463] through the Michael J. Fox Foundation for Parkinson's Research (MJFF). For the purpose of open access, the authors have applied a CC-BY public copyright license to the author accepted manuscript version arising from this submission."

Author Contributions

D.R.A. and A.R.K. designed experiments and supervised the work. D.W., A.R.K., A.K. and K.B. produced recombinant proteins. D.W. and A.R.K. performed crystallization and A.R.K. determined the structures. K.B. designed and carried out cellular and *in vitro* kinetic assays. D.W., K.B., D.R.A and A.R.K. wrote the manuscript.

Conflict of interest

The authors declare that that have no conflict of interest.

Data Availability

The structures of PPM1H phosphatase have been deposited in the Protein Data Bank with codes 7kpr, 7l4j and 7l4i.

References

1. Chen MJ, Dixon JE, Manning G (2017) Genomics and evolution of protein phosphatases. *Science Signaling* **10**: eaag1796

2. Moore F, Weekes J, Hardie DG (1991) Evidence that AMP triggers phosphorylation as well as direct allosteric activation of rat liver AMP-activated protein kinase. *European Journal of Biochemistry* **199**: 691-697

3. Maeda T, Wurgler-Murphy SM, Saito H (1994) A two-component system that regulates an osmosensing MAP kinase cascade in yeast. *Nature* **369**: 242-245

4. Grzechnik AT, Newton AC (2016) PHLPPing through history: a decade in the life of PHLPP phosphatases. *Biochemical Society Transactions* **44**: 1675-1682

5. Vassylyev DG, Symersky J (2007) Crystal structure of pyruvate dehydrogenase phosphatase 1 and its functional implications. *J Mol Biol* **370**: 417-26

6. Linn TC, Pettit FH, Reed LJ (1969) Alpha-keto acid dehydrogenase complexes. X. Regulation of the activity of the pyruvate dehydrogenase complex from beef kidney mitochondria by phosphorylation and dephosphorylation. *Proceedings of the National Academy of Sciences of the United States of America* **62**: 234-241

7. Das AK, Helps NR, Cohen PT, Barford D (1996) Crystal structure of the protein serine/threonine phosphatase 2C at 2.0 A resolution. *EMBO J* **15**: 6798-809

8. Stern A, Privman E, Rasis M, Lavi S, Pupko T (2007) Evolution of the metazoan protein phosphatase 2C superfamily. *J Mol Evol* **64**: 61-70

9. Debnath S, Kosek D, Tagad HD, Durell SR, Appella DH, Acevedo R, Grishaev A, Dyda F, Appella E, Mazur SJ (2018) A trapped human PPM1A-phosphopeptide complex reveals structural features critical for regulation of PPM protein phosphatase activity. *J Biol Chem* **293**: 7993-8008

10. Su J, Forchhammer K (2013) Determinants for substrate specificity of the bacterial PP2C protein phosphatase tPphA from Thermosynechococcus elongatus. *The FEBS Journal* **280**: 694-707

11. Pullen KE, Ng H-L, Sung P-Y, Good MC, Smith SM, Alber T (2004) An Alternate Conformation and a Third Metal in PstP/Ppp, the M. tuberculosis PP2C-Family Ser/Thr Protein Phosphatase. *Structure* **12**: 1947-1954

12. Rantanen MK, Lehtiö L, Rajagopal L, Rubens CE, Goldman A (2007) Structure of Streptococcus agalactiae serine/threonine phosphatase. *The FEBS Journal* **274**: 3128-3137

13. Schlicker C, Fokina O, Kloft N, Grüne T, Becker S, Sheldrick GM, Forchhammer K (2008) Structural Analysis of the PP2C Phosphatase tPphA from Thermosynechococcus elongatus: A

Flexible Flap Subdomain Controls Access to the Catalytic Site. *Journal of Molecular Biology* **376**: 570-581

14. Berndsen K, Lis P, Yeshaw WM, Wawro PS, Nirujogi RS, Wightman M, Macartney T, Dorward M, Knebel A, Tonelli F*, et al.* (2019) PPM1H phosphatase counteracts LRRK2 signaling by selectively dephosphorylating Rab proteins. *Elife* **8**

15. Steger M, Tonelli F, Ito G, Davies P, Trost M, Vetter M, Wachter S, Lorentzen E, Duddy G, Wilson S*, et al.* (2016) Phosphoproteomics reveals that Parkinson's disease kinase LRRK2 regulates a subset of Rab GTPases. *Elife* **5**: e12813

16. West AB, Cookson MR (2016) Identification of bona-fide LRRK2 kinase substrates. *Mov Disord* **31**: 1140-1

17. Alessi DR, Sammler E (2018) LRRK2 kinase in Parkinson's disease. *Science* **360**: 36-37

18. Di Maio R, Hoffman EK, Rocha EM, Keeney MT, Sanders LH, De Miranda BR, Zharikov A, Van Laar A, Stepan AF, Lanz TA*, et al.* (2018) LRRK2 activation in idiopathic Parkinson's disease. *Science Translational Medicine* **10**: eaar5429

19. Hutagalung AH, Novick PJ (2011) Role of Rab GTPases in membrane traffic and cell physiology. *Physiol Rev* **91**: 119-49

20. Dhekne HS, Yanatori I, Gomez RC, Tonelli F, Diez F, Schule B, Steger M, Alessi DR, Pfeffer SR (2018) A pathway for Parkinson's Disease LRRK2 kinase to block primary cilia and Sonic hedgehog signaling in the brain. *Elife* **7**: e40202

21. Holm L (2020) DALI and the persistence of protein shape. *Protein Science* **29**: 128-140

22. Waschbüsch D, Purlyte E, Pal P, McGrath E, Alessi DR, Khan AR (2020) Structural Basis for Rab8a Recruitment of RILPL2 via LRRK2 Phosphorylation of Switch 2. *Structure* **28**: 406-417.e6

23. Bradshaw N, Levdikov VM, Zimanyi CM, Gaudet R, Wilkinson AJ, Losick R (2017) A widespread family of serine/threonine protein phosphatases shares a common regulatory switch with proteasomal proteases. *Elife* **6**

24. Adams PD, Afonine PV, Bunkoczi G, Chen VB, Davis IW, Echols N, Headd JJ, Hung LW, Kapral GJ, Grosse-Kunstleve RW*, et al.* (2010) PHENIX: a comprehensive Python-based system for macromolecular structure solution. *Acta Crystallogr D Biol Crystallogr* **66**: 213-21

25. McCoy AJ, Grosse-Kunstleve RW, Adams PD, Winn MD, Storoni LC, Read RJ (2007) Phaser crystallographic software. *J Appl Crystallogr* **40**: 658-674

26. Emsley P, Lohkamp B, Scott WG, Cowtan K (2010) Features and development of Coot. *Acta Crystallogr D Biol Crystallogr* **66**: 486-501

27. Longo PA, Kavran JM, Kim M-S, Leahy DJ (2013) *Chapter Eighteen - Transient Mammalian Cell Transfection with Polyethylenimine (PEI)*. In Methods in Enzymology, Lorsch J (ed) pp 227-240. Academic Press

28. Fell MJ, Mirescu C, Basu K, Cheewatrakoolpong B, DeMong DE, Ellis JM, Hyde LA, Lin Y, Markgraf CG, Mei H*, et al.* (2015) MLi-2, a Potent, Selective, and Centrally Active Compound for Exploring the Therapeutic Potential and Safety of LRRK2 Kinase Inhibition. *Journal of Pharmacology and Experimental Therapeutics* **355**: 397-409

29. Baykov AA, Evtushenko OA, Avaeva SM (1988) A malachite green procedure for orthophosphate determination and its use in alkaline phosphatase-based enzyme immunoassay. *Analytical Biochemistry* **171**: 266-270

Figure Legends

Figure 1: *Structure of PPM1H phosphatase.* **(A)** Domain organization of PPM1H and PPM1A. The annotation of regions (anchor, flap domain) is discussed in the text. The loop deletion (188-226) that was engineered to improve diffraction is indicated. **(B)** Ribbon model of the enzyme with a view to the catalytic cleft that contains two Mg2+ ions (cyan spheres). The N-terminal region is magenta (33-71), the flap domain is a wheat colour, and the β-sheet motif is green. The back view of the enzyme is also shown with a 180° rotation around the axis indicated. The β1 strand is orange to emphasize its unusual conformation as a consequence of the N-terminal tether (magenta). The side chains of the hydrophobic anchor (RPxFL motif) that interacts with the globular core are shown as stick models, and discussed in the text. **(C)** Comparisons of the flap domain of PPM1H with PPM1A(left) and the tudor domain (right). Apart for a conserved loop (dotted circle) which forms an interface with the catalytic domain, the sequences and structures of the flaps are diverse among the PPM family.

Figure 2: *Docking of pRab8a substrate onto PPM1H and mutagenesis reveal determinants of catalysis*. **(A)** Ribbon model of pRab8a (yellow) docked onto the active site of PPM1H. Phosphorylated T72 (pT72) is shown in sticks at the active site. Residues that were subjected to mutagenesis are marked with red dotted spheres over their side chains. A hydrophobic residue in the conserved loop of the flap domain (L392, dotted circle) is shown as ribbon/stick against the electrostatic surface of the core catalaytic domain (right side). The sequence conservation of this loop is shown below the figure. The black circles represent mutations (single, quadruple) discussed below. **(B)** Kinetics of phosphate hydrolysis by WT and mutant PPM1H. The G domain of pRab8a (1-181, GDP form) was the substrate on left graph, while the T72-phosphorylated switch 2 peptide was the substrate on the right graph. WT and PPM1H (25 nM) were incubated *in vitro* with 16 μM pT72 phosphorylated Rab8a under conditions described in Materials and Methods. Enzyme activity was measured by calculating free phosphate release (*y*-axis) and plotted against time using GraphPad Prism5 software (N=4). For the peptide experiments (right side), 50 nM enzyme and 32 μM peptide was used (N=4). **(C)** HEK293 cells overexpressing indicated constructs were treated ±200 nM MLi-2 for 90 min and then lysed. Mli-2 is a potent inhibitor of LRRK2 and acts as a negative control for detection of phosphoryated Rabs. H153D is an inactive variant of PPM1H and acts as a negative control for dephosphorylation. 10 μg whole cell lysate was subjected to immunoblot analysis with the indicated antibodies at 1 μg/ml final concentration and membranes were analysed using the OdysseyClx Western Blot imaging system. Each lane represents cell extract obtained from a different

dish of cells (two replicates per condition without MLi-2 treatment, one replicate per condition with MLi-2 treatment). **(D)** PPM1H was incubated with increasing concentrations (2-32μM) of (left) pT72 phosphorylated Rab8a[GTPγS bound conformation] (N=2) or (middle) pT72 phosphorylated Rab8a[GDP bound conformation] (N=2) for indicated times as described in **Materials and Methods**. Initial velocity (V_0) was calculated by dividing the concentration of phosphatase (μM) by time (min) and plotted against substrate concentration for (right) pT72 phosphorylated Rab8a[GTPγS bound conformation] (blue) and pT72 phosphorylated Rab8a[GDP bound conformation] (red). Kinetic constants (K_{cat}, V_{max}, K_m) were obtained using GraphPad software. Uncertainties (±) correspond to the standard error of measurements.

Figure 3: *Anchor of PPM1H contributes to folding/catalysis*. **(A)** Interactions between the anchor of PPM1H against the electrostatic surface of the core catalytic domain. The region is placed in context with the dotted box on a ribbon model of PPM1H (right). **(B)** Incremental deletions of the N-terminus from residues 1-37 to 1-44, one residue at a time. The dashed line in the gel indicates the point at which R43 is included (43-end) and the enzyme retains activity. Upon deletion of R43 (44-end), a reduced level of soluble PPM1H expression has no significant catalytic activity. **(C)** Sequence alignment of the N-terminal regions of the evolutionarily related PPM1H/J/M enzymes. The degree of conservation is above the alignment, and residue numbers correspond to PPM1H. A conserved anchor motif (RPxFL) is annotated below the sequences.

Figure 4: *Sequence and structural comparisons of PPM1H and PPM1J suggest Rab specificity lies outside of the catalytic domain.* **(A)** Domain comparisons of PPM1H and PPM1J. Apart from flexible loops that are distant from the active site (indicated in parentheses), the two enzymes are similar. **(B)** Heat map of PPM1H/J sequence diversity superimposed onto the ribbon model of PPM1H. The rectangular bar displays the variation from low (red) to high (blue) sequence identities.

Figure 5: *Domain swapped chimera of PPM1J with PPM1H flap acquires catalytic activity against pRab8a.* **(A)** Chimeras of PPM1J and their notation for *in vitro* kinetics data. **(B)** Purity of recombinant proteins used for assays. 3 μg of WT PPM1J or PPM1J chimera proteins were resolved on 4-12% Bis-Tris gradient gel and stained with Instant Blue Coomassie. **(C)** Recombinant enzymes were incubated *in vitro* with 16 μM pRab8a-GTPγS (*left*) or 32 μM phospho-peptide (*right*) and the release of phosphate was measured as decribed in **Materials and Methods**. **(D)** Model for substrate specificity of PPM1H. Phosphorylated switch 2 helix of a model Rab is yellow. The flap domain

encodes specificity for phosphorylated Rabs while the anchor contributes to folding and catalysis. The conserved loop motif marked by L392 of the flap domain may couple substrate binding to catalysis.

Table 1. PPM1H Crystallographic Data and Refinement Statistics			
	D288A	WT^{LD}	$D288A^{LD}$
PPM1H residues	33-514	33-514	33-514
Crystallization	10% isopropanol, 5% PEG4000, 0.05M $MgCl_2$	0.1M imidazole pH 7, 20% Jeffamine ED-2001	30% PEG1500 0.1M MES pH 6.5
Beamline	NSLSII FMX	NSLSII FMX	NSLSII FMX
Wavelength (Å)	0.9789	0.9789	0.9789
Space group	$P\ 2_1\ 2_1\ 2_1$	$P\ 2_1\ 2_1\ 2_1$	$P\ 2_1\ 2_1\ 2_1$
Cell a, b, c, (Å)	69.68 102.16 148.70	71.31, 102.4, 148.72	70.69, 101.11, 148.97
Resolution (Å)	28.55–3.09 (3.20-3.09)	28.97–2.45 (2.54–2.45)	28.97–2.58 (2.68-2.58)
Unique reflections	19,927 (1,853)	39,279 (3,324)	34,031 (3,228)
Completeness (%)	99.25 (95.02)	98.28 (84.34)	99.42 (96.04)
$\langle I/\sigma \rangle$	19.83 (2.34)	14.6 (2.3)	16.79 (0.35)
Multiplicity	6.7 (6.3)	6.7 (6.7)	6.6 (6.5)
R-merge	0.070 (0.77)	0.08 (0.78)	0.0897 (0.673)
R-meas	0.076 (0.0.84)	0.086 (0.855)	0.097 (0.731)
$CC_{1/2}$	0.999 (0.855)	0.998 (0.779)	0.998 (0.847)
Refinement			
Protein residues/waters/Mg^{2+}	794/14/4	793/115/4	794/91/4
No. reflections for R-free	1003 (85)	1,968 (166)	1,708 (171)
R-work	0.1878 (0.3349)	0.1824 (0.2684)	0.1897 (0.2441)
R-free	0.2148 (0.4032)	0.2389 (0.3428)	0.2359 (0.2908)
RMSD bond lengths (Å)	0.005	0.009	0.004
RMSD bond angles (°)	0.96	1.07	0.78
Average overall *B*-factor	98.78	61.03	57.65
Mean B-factors ($Å^2$) protein/waters/Mg^{2+}	98.83/86.73/81.95	61.15/54.83/44.09	57.67/56.62/56.31
Ramachandran analysis favored/allowed (%)	94.63/4.48	95.5/3.86	96.53/3.08
PDB accession code	7kpr	7l4j	7l4i

Values in parentheses correspond to the statistics in the highest resolution bin. RMSD, root-mean-square deviation. LD corresponds to the 'loop deletion' variant of PPM1H.

R-merge = $\Sigma_{hkl} \Sigma_j \left| I_{hkl,j} - \langle I_{hkl} \rangle \right| / \Sigma_{hkl} \Sigma_{jhkl,j}$

R-work = $\Sigma_{hkl} \left| F_{o,hkl} - F_{c,hkl} \right| / \Sigma_{hkl} F_{o,hkl}$

Expanded View Figure Legends

Figure EV1: *Cellular activity of 'loop deletion' variant of PPM1H and sequence alignment of the PPM family.* **(A)** HEK293 cells overexpressing indicated constructs were treated with ±200 nM MLi-2 (inhibitor of LRRK2 kinase) for 90 min and then lysed. Whole cell lysate (10 μg) was subjected to immunoblot analysis with the indicated antibodies at 1 μg/ml final concentration. Each lane represents cell extract obtained from two different dishes of cells without MLi-2 treatment, one replicate per condition with MLi-2 treatment. D288A and D221A are phosphatase-dead variants. The 'loopDEL' variant is the segment 33-514 with the region 188-226 replaced by the sequence 'GSGS'. **(B)** Structure-based sequence alignment of human PPMs. Secondary structures of PPM1H and PPM1A are above and below the sequences, respectively. Colours of secondary structures correspond to the scheme in Fig 1. The black triangle is a loop in PPM1H (188-226) that has been removed to simplify the alignment. The C-terminal α-helical domain of PPM1A is blue. Red circles are aspartate residues that directly coordinate metal ions.

Figure EV2: *Purification of recombinant proteins and cellular assay of WT and mutant PPM1H activity.* **(A)** PPM1H variants were purified as SUMO-tagged fusions as described in Materials and Methods. 3 μg of recombinant wild-type or indicated mutant PPM1H proteins were resolved on 4-12% Bis-Tris gradient gel and stained with Instant Blue Coomassie. L392A variant was less pure relative to WT and other mutants, therefore it was not used for quantitative kinetics assays. **(B)** HEK293 cells overexpressing indicated constructs were treated with ±200 nM MLi-2 were analyzed for pRab10 levels as described in **Materials and Methods**. Each lane represents cell extract obtained from a different three different dish of cells per condition (one replicate with MLi-2 treatment). The triple mutant comprising the anchor motif is not expressed solubly. Single L392A mutant and the quadruple (L393A+D39A+H395A+D396A) in a conserved loop from the flap domain are partially/fully defective in pRab10 hydrolysis, suggesting their contribution to catalysis. R338A in the flap domain also shows a partial defect despite its distance (27 Å) from the active site.

Figure EV4: Sequence alignment of PPM1H and PPM1J. The secondary structure of PPM1H is annotated above the sequences. The anchor and the flap domain are shown with lightly shaded rectangles. These segments were swapped to generate the PPM1J chimeras.

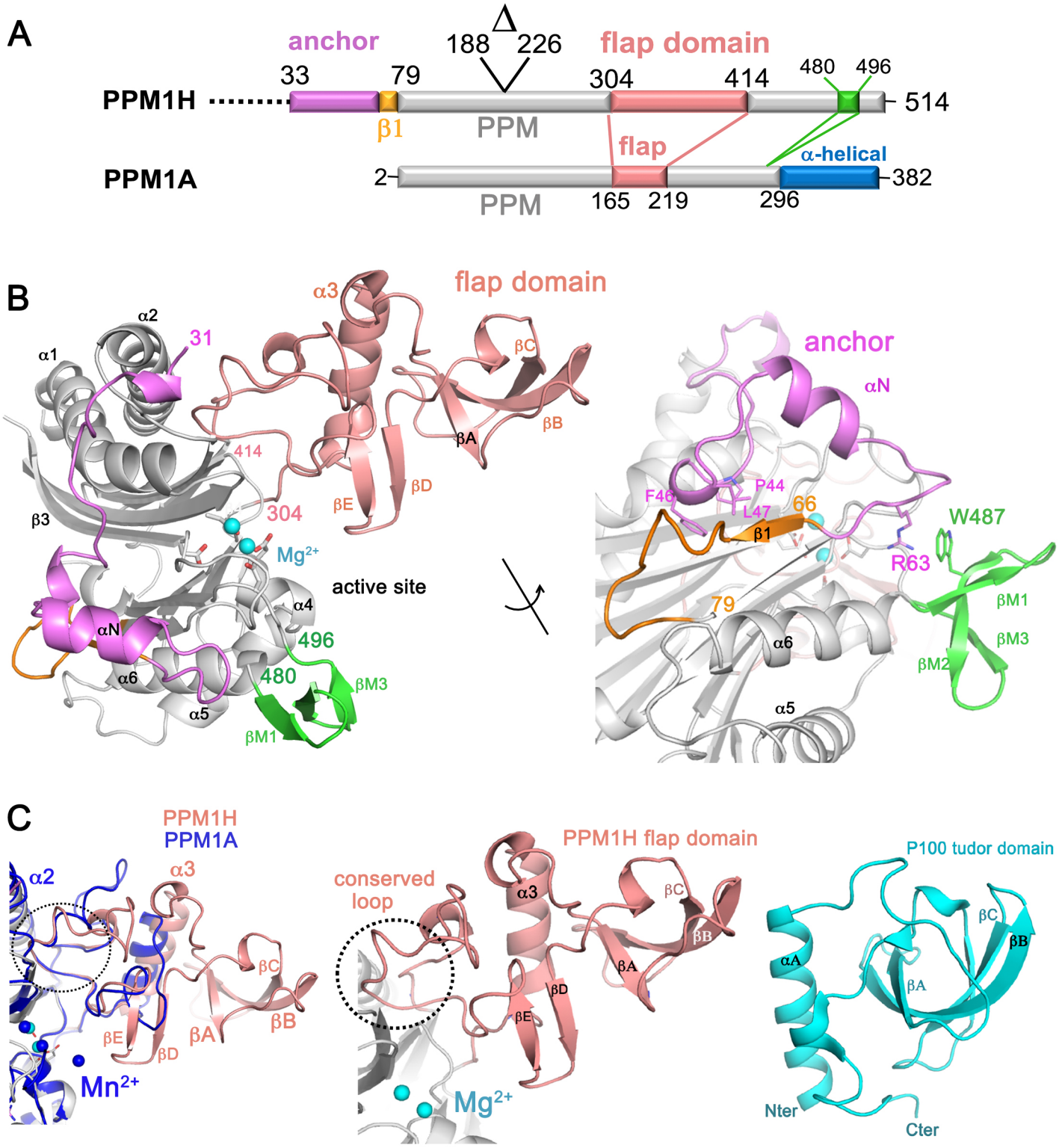
A
anchor
Δ
188
226
flap domain
33
79
304
414
480
496
PPM1H
514
β1
PPM
flap
α-helical
PPM1A
2
382
PPM
165
219
296
B
α3
flap domain
α2
31
α1
βC
βB
βA
414
βD
βE
304
β3
Mg2+
active site
α4
αN
496
α6
480
βM3
α5
βM1
anchor
αN
F46
P44
L47
66
β1
W487
R63
79
βM1
βM3
α6
βM2
α5
C
PPM1H
PPM1A
α2
α3
βC
βE
βA
βB
βD
Mn2+
conserved
loop
PPM1H flap domain
α3
βC
βB
βA
βD
βE
Mg2+
P100 tudor domain
βC
βB
αA
βA
Nter
Cter

Figure 1

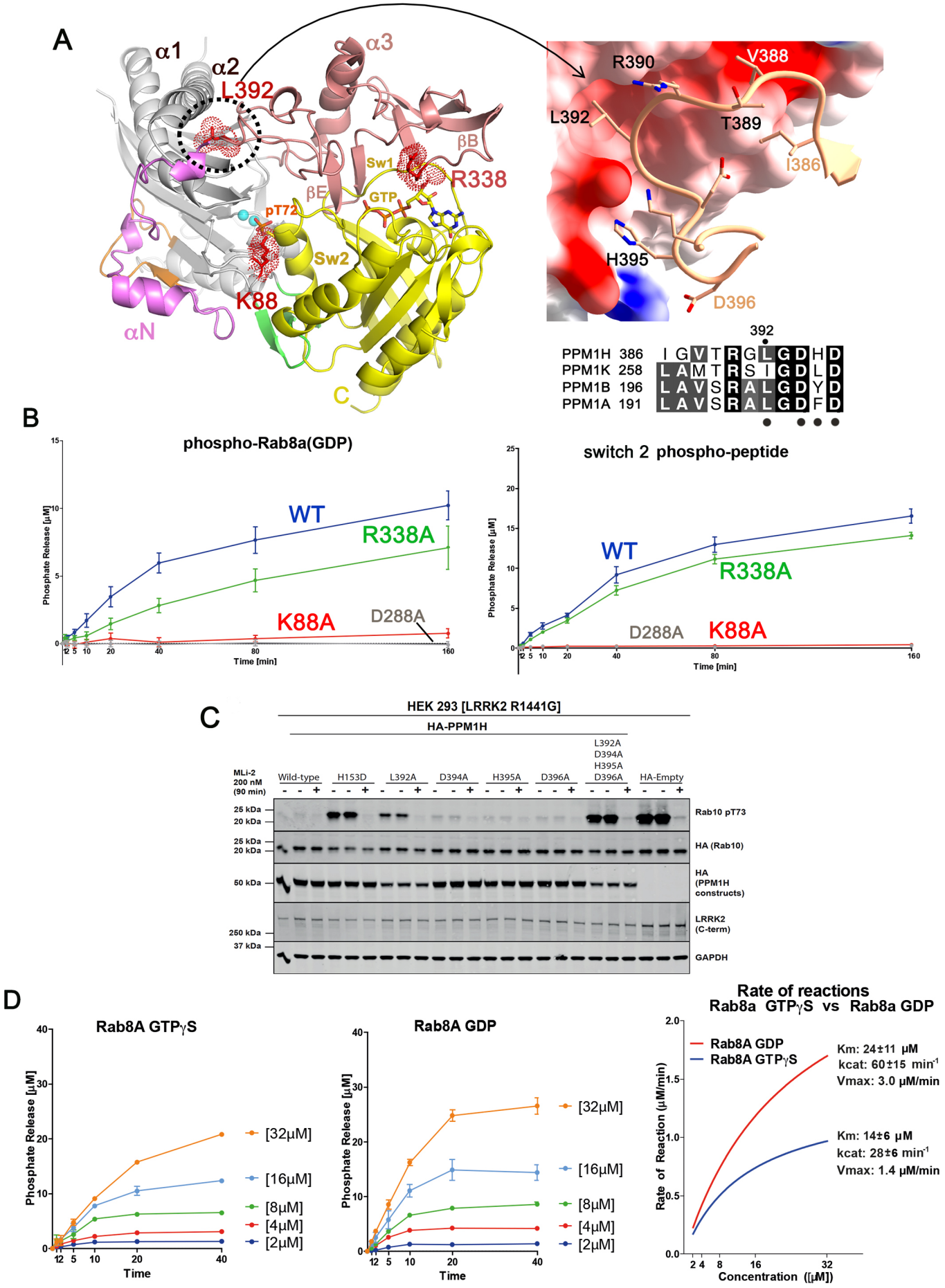
A
α1
α2
L392
α3
βB
Sw1
R338
βE
GTP
pT72
Sw2
K88
αN
C
R390
V388
L392
T389
I386
H395
D396
392
PPM1H 386 I G V T R G L G D H D
PPM1K 258 L A M T R S I G D L D
PPM1B 196 L A V S R A L G D Y D
PPM1A 191 L A V S R A L G D F D
B
phospho-Rab8a(GDP)
Phosphate Release [μM]
Time [min]
WT
R338A
K88A
D288A
switch 2 phospho-peptide
Phosphate Release [μM]
Time [min]
WT
R338A
D288A
K88A
C
HEK 293 [LRRK2 R1441G]
HA-PPM1H
MLi-2 200 nM (90 min)
Wild-type
H153D
L392A
D394A
H395A
D396A
L392A D394A H395A D396A
HA-Empty
25 kDa
20 kDa
Rab10 pT73
HA (Rab10)
50 kDa
HA (PPM1H constructs)
250 kDa
37 kDa
LRRK2 (C-term)
GAPDH
D
Rab8A GTPγS
Phosphate Release [μM]
Time
[32μM]
[16μM]
[8μM]
[4μM]
[2μM]
Rab8A GDP
Phosphate Release [μM]
Time
[32μM]
[16μM]
[8μM]
[4μM]
[2μM]
Rate of reactions
Rab8a GTPγS vs Rab8a GDP
Rab8A GDP
Rab8A GTPγS
Km: 24±11 μM
kcat: 60±15 min-1
Vmax: 3.0 μM/min
Km: 14±6 μM
kcat: 28±6 min-1
Vmax: 1.4 μM/min
Rate of Reaction (μM/min)
Concentration ([μM])

Figure 2

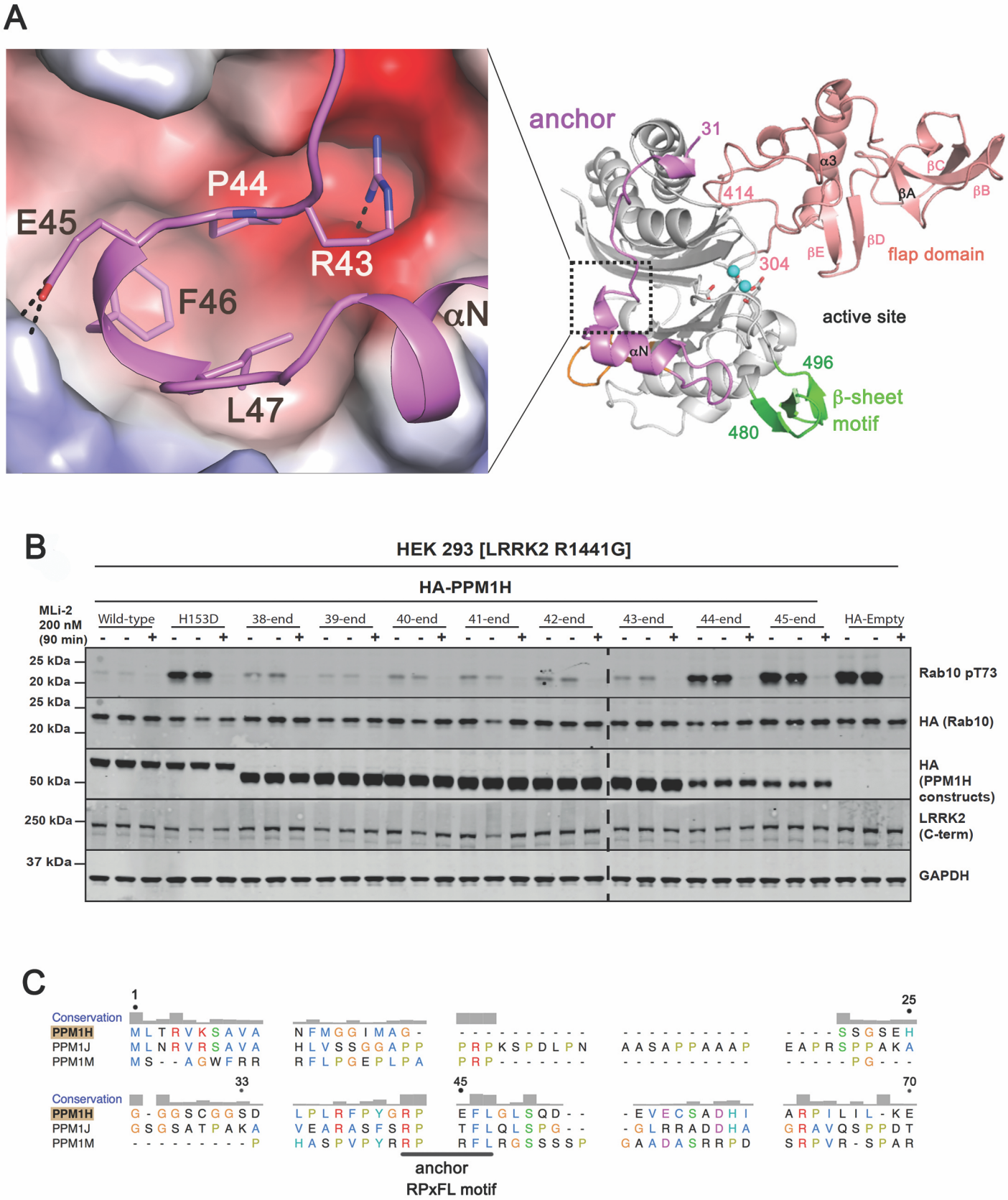
A
P44
E45
R43
F46
αN
L47
anchor
31
414
α3
βC
βA
βB
βE
βD
flap domain
304
active site
αN
496
β-sheet
motif
480
B
HEK 293 [LRRK2 R1441G]
HA-PPM1H
MLi-2
200 nM
(90 min)
Wild-type
H153D
38-end
39-end
40-end
41-end
42-end
43-end
44-end
45-end
HA-Empty
25 kDa
20 kDa
25 kDa
20 kDa
50 kDa
250 kDa
37 kDa
Rab10 pT73
HA (Rab10)
HA
(PPM1H
constructs)
LRRK2
(C-term)
GAPDH
C
Conservation
PPM1H
PPM1J
PPM1M
anchor
RPxFL motif

Figure 3

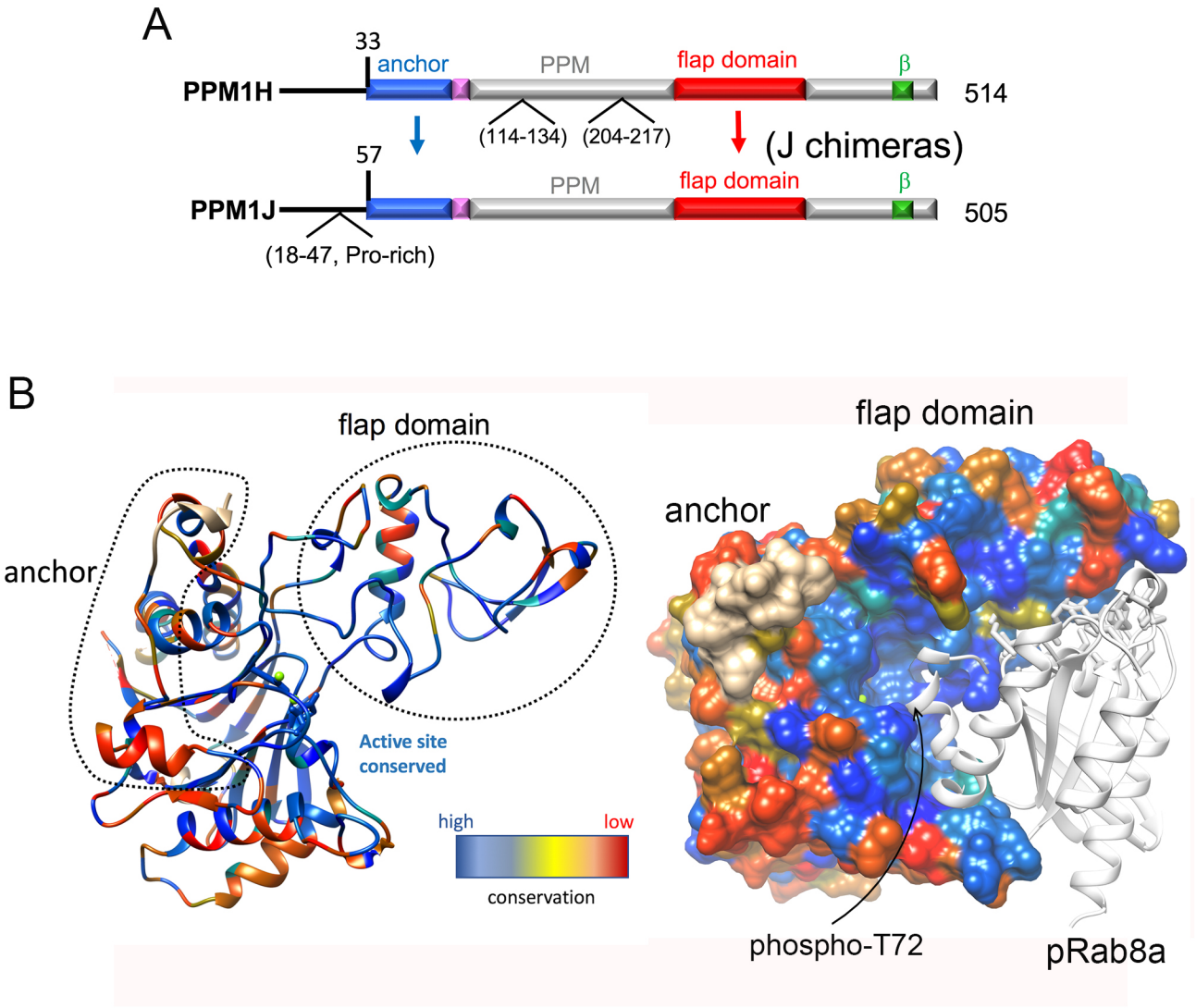
A
33
anchor
PPM
flap domain
β
PPM1H
514
(114-134)
(204-217)
(J chimeras)
57
PPM
flap domain
β
PPM1J
505
(18-47, Pro-rich)
B
flap domain
anchor
Active site
conserved
high
low
conservation
flap domain
anchor
phospho-T72
pRab8a

Figure 4

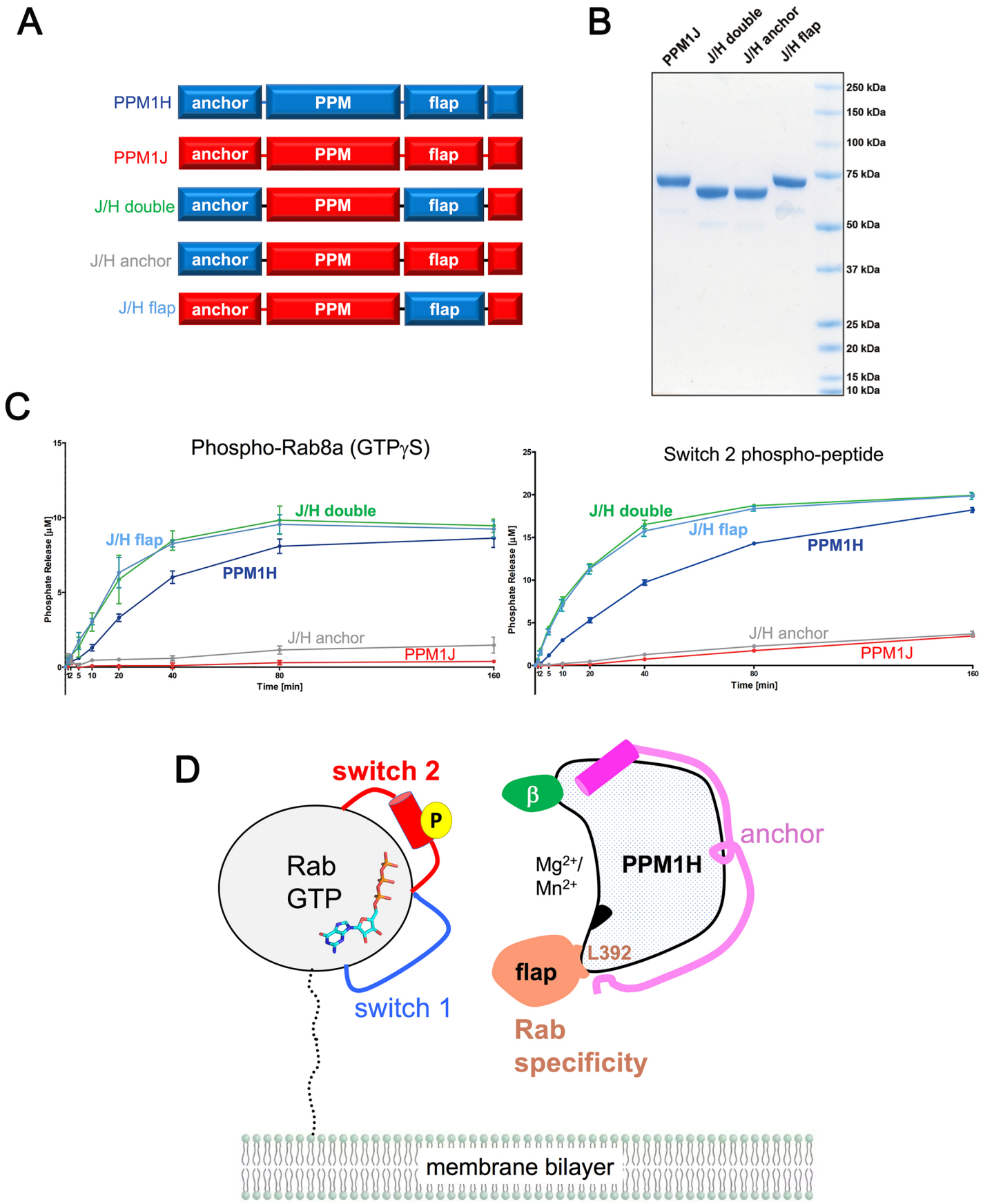
A
PPM1H
anchor
PPM
flap
PPM1J
J/H double
J/H anchor
J/H flap
B
PPM1J
J/H double
J/H anchor
J/H flap
250 kDa
150 kDa
100 kDa
75 kDa
50 kDa
37 kDa
25 kDa
20 kDa
15 kDa
10 kDa
C
Phospho-Rab8a (GTPγS)
Phosphate Release [µM]
Time [min]
J/H double
J/H flap
PPM1H
J/H anchor
PPM1J
Switch 2 phospho-peptide
D
switch 2
P
Rab
GTP
switch 1
β
Mg2+/
Mn2+
PPM1H
anchor
L392
flap
Rab
specificity
membrane bilayer

Figure 5